

Circumstellar Dust Features as seen by ISO/SWS

Yamamura Issei (ISAS) *yamamura@ir.isas.ac.jp*

00/11/29

Prepared for ISO Spectroscopic Workshop on 2000 Dec. 6

1 Crystalline Silicates

1.1 Detections

- AGB/post-AGB/PNe : Waters et al. (1996) (Fig.1)
- YSO's : Waelkens et al. (1996), Malfait et al. (1999)
- Comet Hale-Bopp : Crovisier J., et al. (1997)

1.2 Properties

- Identification: Olivines ($\text{Mg}_{2x}\text{Si}_{2-2x}\text{O}_4$), Piroxines ($\text{Mg}_x\text{Si}_{1-x}\text{O}_3$).
- Almost completely Mg-rich ($x \approx 1$): Jäger et al. (1998), Molster et al. (1999a) (Fig.2).
- ≤ 20 per cent of silicate dust is crystalline in the AGB mass-loss wind (Molster et al. 1999a).
- Fraction of crystalline silicate increases with the mass-loss rate? Not necessary (Kamper et al. 2001).

1.3 Disk Sources

- Some post-AGB objects show exceptionally strong crystalline silicate features (e.g. IRAS 09425–6040, Molster et al. 2001) (Fig.3).
- Also a few YSO's exhibit strong crystalline silicate features (e.g. HD 100546, Waelkens et al. 1996).
- IRAS 09425–6040 and the Red Rectangle (Waters et al. 1998) show both oxygen-rich and carbon-rich nature.
- These sources are known to have circumstellar disks, therefore, presence of disk may enhance the crystallinity.

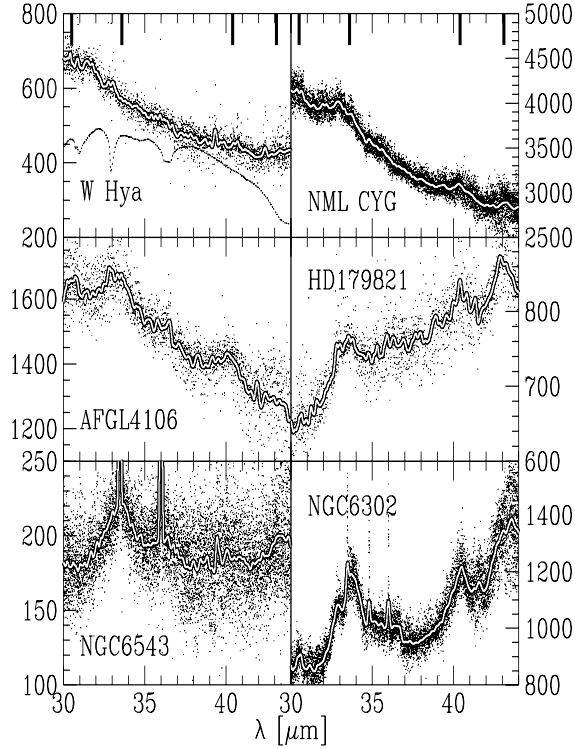


Figure 1: The SWS spectra of AGB stars, post-AGB objects, and Planetary Nebulae in the wavelength range between 30–45 μm . The crystalline silicate features indicated with ticks appear more prominently in the later evolutionary phase. The Relative Spectral Responsivity Function (RSRF) is plotted together with W Hya in order to show that these features are not due to calibration error (Waters et al. 1996).

1.4 Formation Process

- Thermal annealing: A few hours at ~ 1030 K produces crystalline silicates, but this time scale is a very steep function of the annealing temperature (Hallenbeck et al. 2000).
- Possibility of athermal annealing process are proposed (Molster et al. 1999b).

2 Carbon-rich dust

2.1 UIR (PAH) bands

- UIR (PAH) features in broad infrared wavelengths: Beintema et al. (1996) (Fig.4).
- Systematic study of the evolution of the features are ongoing (Hony et al. in preparation).

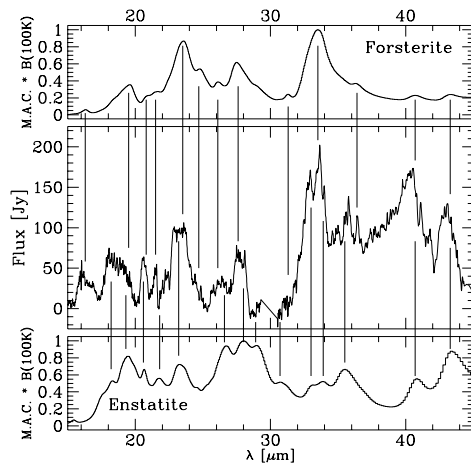


Figure 2: The SWS spectrum of the post-AGB star, AFGL 4106 is compared with forsterite and clinoenstatite at 100 K. Most of crystalline silicate features in AFGL 4106 can be identified with these two minerals. From Jäger et al. (1998).

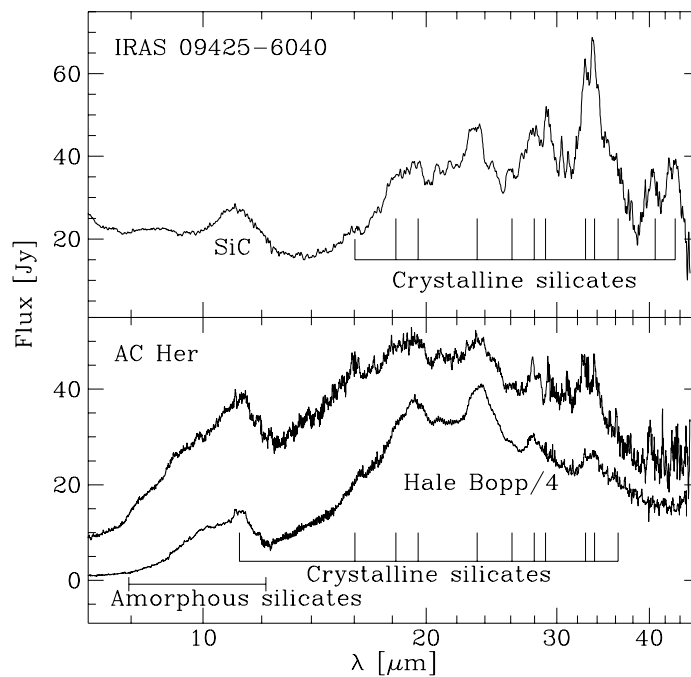


Figure 3: *Upper*: The SWS spectrum of the carbon star IRAS 09425–6040. The star shows the most prominent crystalline silicate features of all the objects observed by ISO. About 75 per cent of silicates are crystalline. *Lower*: The SWS spectrum of the post-AGB object AC Her is compared with that of comet Hale-Bopp. The similarity of the two spectra is remarkable. The figure is taken from Molster et al. (1999b).

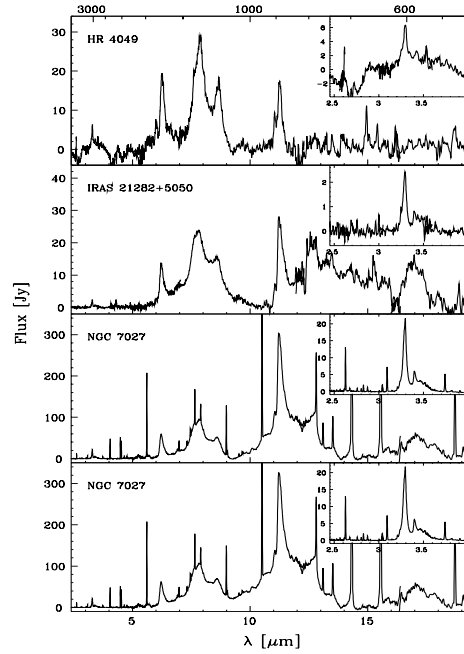


Figure 4: UIR (PAH) features observed by ISO/SWS in post-AGB object / Planetary Nebula (Beintema et al. 1996).

2.2 30 μm feature

- Commonly exists in carbon-rich AGB stars with optically thick circumstellar envelope : Yamamura et al. (1998) (Fig.5).
- Systematic study of the evolution of the features are ongoing :Hony et al. (in preparation).
- Sub-structure / multi components? : Sczcerba et al. (1999), Hony et al. (in preparation = MgS + Graphite?).

2.3 21 μm feature

- Only appears in metal-poor, C-rich post-AGB objects with the spectral types of G or F.
- All objects show the same *intrinsic* profile : Volk et al. (1999) (Fig.6)
- Identification (?) with TiC : von Helden et al. (2000) (Fig.7)

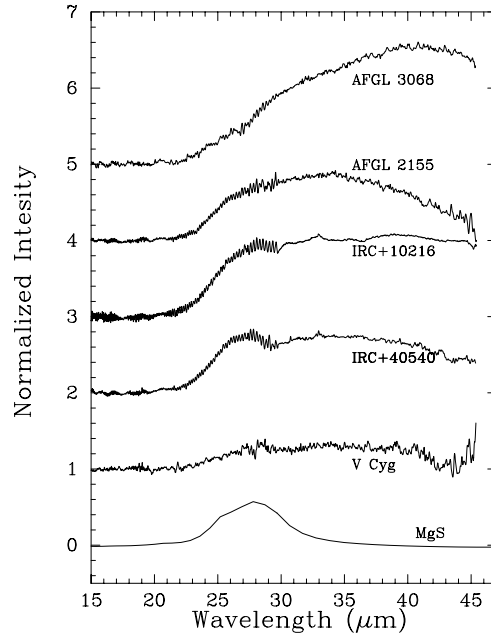


Figure 5: Spectra of five carbon stars normalized with “continuum” extrapolated from the shorter wavelengths. The mass-loss rate increases from bottom (V Cyg) to top (GL 3068). The feature evolves with the increasing mass-loss rate. The lowest line shows the opacity of MgS. It is seen that MgS itself cannot explain the whole feature. (see also Yamamura et al. 1998).

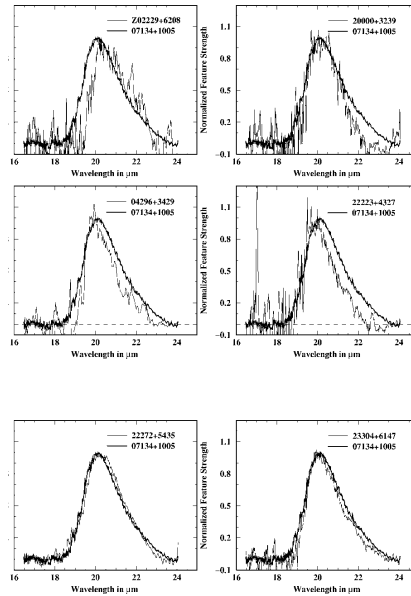


Figure 6: Normalized spectra of $21 \mu\text{m}$ feature in 6 post-AGB objects compared with that of IRAS 07134+1005.

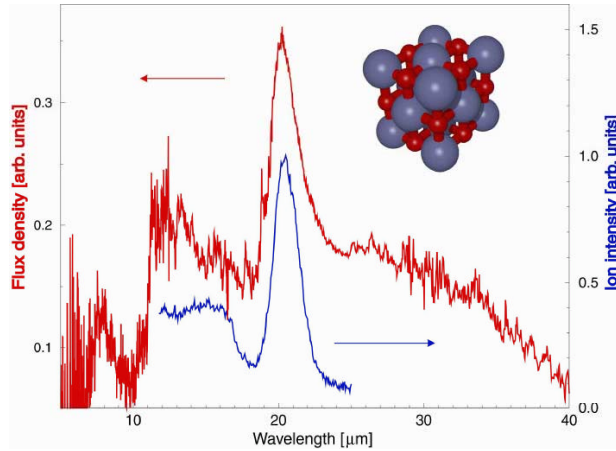


Figure 7: Comparison of the ISO/SWS spectrum of the post-AGB object SAO 96709 with the laboratory spectrum of TiC nanocrystal clusters. The measurement was done by the electron energy loss spectroscopy (EELS) method. Right-top is a pictorial representation of a typical ($4 \times 4 \times 4$ atom) TiC nanocrystal (carbon: red, Ti: blue).

REFERENCES

- Beintema D.A. et al. 1996, A&A 315, L369
 Crovisier J., 1997, Science 275, 1904
 Hallenbeck S.L., 2000, ApJ 535, 247
 Jäger C. 1998, A&A 339, 904
 Kamper F. 2001, A&A submitted
 Molfait K. et al. 1999, A&A 345, 181
 Molster F.J. et al. 1999a, A&A 350, 163
 Molster F.J. et al. 1999b, Nature 401, 563
 Molster F.J. et al. 2001, A&A, in press
 von Helden G. et al. 2000, Science 288, 313
 Volk K. et al. 2000, ApJ 516, L99
 Waelkens C. et al. 1996, A&A 315, L245
 Waters L.B.F.M. et al. 1996, A&A 315, L361
 Yamamura I. et al. 1998, ApSS 225, 351